

# Localization-enhanced moiré exciton in twisted transition metal dichalcogenide heterotrilayer superlattices

Yanping LIU (✉ [liyuanping@csu.edu.cn](mailto:liyuanping@csu.edu.cn))

Central South University <https://orcid.org/0000-0003-2990-3783>

Haihong Zheng

Central South University

Biao Wu

Central South University

Shaofei Li

Central South University

Junnan Ding

Central South University

Jun He

Central South University

Zongwen Liu

The University of Sydney <https://orcid.org/0000-0002-6434-1643>

Chang-Tian Wang

Institute of Physics, Chinese Academy of Sciences

Jian-Tao Wang

Institute of Physics, Chinese Academy of Sciences

Anlian Pan

Hunan University <https://orcid.org/0000-0003-3335-3067>

---

## Article

### Keywords:

**Posted Date:** September 14th, 2022

**DOI:** <https://doi.org/10.21203/rs.3.rs-2037324/v1>

**License:**   This work is licensed under a Creative Commons Attribution 4.0 International License.

[Read Full License](#)

---

# Localization-enhanced moiré exciton in twisted transition metal dichalcogenide heterotrilinear superlattices

Haihong Zheng<sup>1,2</sup>, Biao Wu<sup>1,2</sup>, Shaofei Li<sup>1</sup>, Junnan Ding<sup>1</sup>, Jun He<sup>1</sup>, Zongwen Liu<sup>3,4</sup>,  
Chang-Tian Wang<sup>5,6,7</sup>, Jian-Tao Wang<sup>5,6,7</sup>, Anlian Pan<sup>8,\*</sup> & Yanping Liu<sup>1,2,9\*</sup>

1. *School of Physics and Electronics, Hunan Key Laboratory for Super-microstructure and Ultrafast Process, Central South University, 932 South Lushan Road, Changsha, Hunan 410083, People's Republic of China*
2. *State Key Laboratory of High-Performance Complex Manufacturing, Central South University, 932 South Lushan Road, Changsha, Hunan 410083, People's Republic of China*
3. *School of Chemical and Biomolecular Engineering, The University of Sydney, NSW 2006, Australia*
4. *The University of Sydney Nano Institute, The University of Sydney, NSW 2006 Australia*
5. *Beijing National Laboratory for Condensed Matter Physics, Institute of Physics, Chinese Academy of Sciences, Beijing 100190, China*
6. *School of Physical Sciences, University of Chinese Academy of Sciences, Beijing 100049, China*
7. *Songshan Lake Materials Laboratory, Dongguan, Guangdong 523808, China*
8. *Hunan Institute of Optoelectronic Integration, College of Materials Science and Engineering, Hunan University, Changsha, Hunan 410082, People's Republic of China*
9. *Shenzhen Research Institute of Central South University, A510a, Shenzhen. People's Republic of China*

## Abstract

Moiré superlattice created by the stacking of twisted 2D layered materials have become a new platform for the study of quantum optics. The strong coupling of moiré superlattices can generate flat minibands that enhance electronic interactions and produce a variety of fascinating strongly correlated states such as non-conventional superconductivity, Mott insulating states and moiré excitons. However, the influence between the adjustment and localization of moiré excitons in Van der Waals heterostructures has not been the subject of experimental investigations. Here we report experimental evidence of the localization-enhanced moiré excitons in the twisted WSe<sub>2</sub>/WS<sub>2</sub>/WSe<sub>2</sub> heterotrilinear with type-II band alignments. At low temperature, we observed multiple excitons splitting phenomena in the twisted WSe<sub>2</sub>/WS<sub>2</sub>/WSe<sub>2</sub> heterotrilinear, manifesting as multiple sharp emission lines, contrasting strongly with the moiré excitonic behavior of the twisted WSe<sub>2</sub>/WS<sub>2</sub> heterobilayer (the linewidth is 4 times narrower). This is primarily because the enhancement of the two moiré potentials in the twisted heterotrilinear enables the moiré excitons at the highly localized interface. Furthermore, the changes in temperature, laser power and valley polarization further demonstrate the confinement effect of moiré potential on moiré excitons. Our findings provide a new way for the localization of moiré excitons in twist-angle heterostructures, facilitating the development of coherent quantum light emitters.

---

\* Correspondence and requests for materials should be addressed to Email:

[liuyanping@csu.edu.cn](mailto:liuyanping@csu.edu.cn); [anlian.pan@hnu.edu.cn](mailto:anlian.pan@hnu.edu.cn)

## Introduction

Recently, the twisted van der Waals heterostructured superlattices have attracted significant attention as they provide a powerful and attractive platform for exploring the new physics of novel condensed matter<sup>1-6</sup>. Vertically stacked 2D materials can generate periodic moiré superlattices due to lattice mismatches or twist angles<sup>7</sup>. The moiré potential in the moiré superlattice dominates the kinetic energy within the mini-Brillouin zone, which changes the electronic band structure in the heterojunction<sup>8-10</sup>, and induces strongly correlated quantum phenomena: including strongly correlated insulators<sup>11-14</sup>, superconductivity<sup>15</sup>, moiré excitons<sup>16-18</sup>, moiré phonons<sup>19,20</sup>, magnetism<sup>21</sup>. Moiré superlattices in twisted two-dimensional (2D) material heterojunctions offer opportunities for the development of many-body physics<sup>22, 23</sup>, which will help to drive the development of novel quantum devices<sup>24</sup>.

The periodic moiré potentials induced by moiré superlattices in van der Waals heterojunctions can trap interlayer excitons to generate moiré exciton arrays<sup>25-27</sup>. The tunability of the moiré potential opens a new avenue for quantum manipulation of quasiparticles in quantum optics. Recently, the moiré excitons have been reported in a twisted MoSe<sub>2</sub>/WSe<sub>2</sub> heterojunction, and multiple interlayer exciton resonance phenomena have been observed. They attribute these resonances to the state of exciton on the ground and the state of excitation related to moiré potential<sup>28</sup>. Such moiré superlattices can be applied to quantum emitter arrays<sup>29</sup>. However, the relationship between the modulation effect of moiré superlattices on the properties of moiré excitons and the number of twisted layers has yet to be further studied, particularly for 2D twisted angle heterojunctions with more than two layers.

In this work, we utilize the layer degrees of freedom to investigate the localization of moiré excitons. We report the observation of multiple exciton resonances in a high-quality hexagonal boron nitride (hBN)-encapsulated in the twisted heterotrilaier. The WSe<sub>2</sub>/WS<sub>2</sub>/WSe<sub>2</sub> heterotrilaier has two type-II band alignments that form two overlapping moiré potentials at the twisted WSe<sub>2</sub>/WS<sub>2</sub> interface. The synergy of the two moiré potentials enables the moiré excitons at the interface very localized, manifesting in the form of multiple sharp emission lines, in sharp contrast to the moiré excitonic behavior of the twisted WSe<sub>2</sub>/WS<sub>2</sub> heterobilayer. Additionally, comparing the variation of the laser power and

temperature of the twisted-angle heterojunction with different layers, further proved that the formation of double moiré fringes at the  $\text{WSe}_2/\text{WS}_2/\text{WSe}_2$  heterotrilinear interface will induce a deeper and narrower moiré potential to localize excitation. Our results offer a new way to regulate the localization of moiré excitons in twisted-angle heterostructures, promising single-photon emission of excitons to advance the application of moiré superlattices in quantum devices.

## 2. Results and Discussion

### 2.1. Schematic and $\text{WSe}_2/\text{WS}_2/\text{WSe}_2$ Heterotrilinear

In the twisted heterostructures of 2D materials, the periodic moiré superlattices can be formed by tuning the lattice mismatch and the interlayer twist angle ( $\theta$ ). The periodicity of the moiré superlattice changes correspondingly with the twist angles, and its electronic structure and energy band structure also changes, resulting in multiple planar exciton miniature energy bands. Moiré exciton bands provide a novel platform for exploring and controlling excited states of matter. Figure 1a shows the schematic of the h-BN-encapsulated  $\text{WSe}_2/\text{WS}_2/\text{WSe}_2$  heterotrilinear, which includes three different regions in the same device: 1L- $\text{WSe}_2$ , 1L- $\text{WSe}_2/\text{WS}_2$  and  $\text{WSe}_2/\text{WS}_2/\text{WSe}_2$  heterotrilinear. The  $\text{WSe}_2/\text{WS}_2/\text{WSe}_2$  heterotrilinear have two type II band alignment, which results in the formation of spatially indirect interlayer excitons, with electrons and holes that reside in the  $\text{WS}_2$  and  $\text{WSe}_2$  layers, respectively (Figure 1b). At the same time, the twisted  $\text{WSe}_2/\text{WS}_2/\text{WSe}_2$  heterotrilinear is a system composed of two-layer  $\text{WSe}_2$  and one-layer  $\text{WS}_2$ . The top and bottom sheets are aligned, and the middle sheet is rotated by a  $\theta$  angle of approximately  $3^\circ$  relative to the other two sheets. Interlayer torsion angles create periodic moiré superlattices at the interface that trap and spatially confine excitons. In the twisted  $\text{WSe}_2/\text{WS}_2/\text{WSe}_2$  heterotrilinear, the torsion angle of the three layers will generate two periodic moiré fringes and then form super moiré fringes, leading to new quantum phenomena.

Figure 1c shows the optical image of the  $\text{WSe}_2/\text{WS}_2/\text{WSe}_2$  heterotrilinear, we can distinguish monolayer, bilayer twist areas and trilinear twist areas. The vdW heterostructures were prepared via polymethyl methacrylate (PMMA)-assisted transfer method. Our

heterobilayer samples encapsulated by hexagonal boron nitride (hBN) (Supplementary Fig. 1). The Raman mapping (Figure 1d) was used to confirm the quality of the twisted  $\text{WSe}_2/\text{WS}_2/\text{WSe}_2$  heterotrילayer. The uniformity of Raman mapping signal intensity can confirm spatial homogeneity over the micrometre length scale, which is mainly attributed to our dry transfer method and annealing treatment. At the same time, the Raman spectra of the heterostructures with different layers further proved that the twisted  $\text{WSe}_2/\text{WS}_2/\text{WSe}_2$  heterotrילayer was successfully prepared (Supplementary Fig. 2). As shown in Figure 1e, the PL spectra of  $\text{WSe}_2/\text{WS}_2/\text{WSe}_2$  heterotrילayer with different layers at room temperature, and it can be found that the PL peak has a red shift and that its intensity decreases with the increase of the number of layers. Also, the PL spectra display a new emission peak at  $\sim 1.52$  eV in the  $\text{WSe}_2/\text{WS}_2/\text{WSe}_2$  heterotrילayer with twist angles of  $3^\circ$ , which is attributed to the emission from the interlayer excitons. The relative twist angle between the top and middle sheets of the sample was determined optically using polarization-dependent second-harmonic-generation measurements<sup>30</sup>. Fig. 1f shows the polarization-dependent PL of the top and a middle sheet of  $\text{WSe}_2$  and  $\text{WS}_2$ , from which can determine a rotation of the principal axis of  $3^\circ \pm 0.2^\circ$  between the layers.

## 2.2. Moiré exciton localization in a $\text{WSe}_2/\text{WS}_2/\text{WSe}_2$ Heterotrילayer

In twisted heterostructures of 2D materials, by adjusting the lattice mismatch and the interlayer twist angle ( $\theta$ ), a moiré superlattice can be formed, resulting in a periodic moiré potential to trap excitons. The  $\text{WSe}_2/\text{WS}_2/\text{WSe}_2$  heterotrילayer has two type-II band alignments, with the conduction band minimum located in the  $\text{WS}_2$  layer and the valance band maximum in the top and bottom  $\text{WSe}_2$  layer. When the top and bottom  $\text{WSe}_2$  layers are slightly misaligned with the middle  $\text{WS}_2$  layer, two interfering moiré patterns are formed at the  $\text{WSe}_2/\text{WS}_2$  interface (Figure 2a). The moiré superlattice leads to band folding in the mini-Brillouin region and creates moiré exciton bands that capture more moiré excitons<sup>31</sup>. The synergy of the two moiré potentials enables the moiré excitons at the interface highly localized (Figure 2b).

To investigate the localized effects of the layer degree of freedom on moiré excitons, we performed micro-photoluminescence measurements on the twisted  $\text{WSe}_2/\text{WS}_2$  heterobilayer and the  $\text{WSe}_2/\text{WS}_2/\text{WSe}_2$  heterotrilevel at 6 K under a low excitation power. The PL spectrum of 1L- $\text{WSe}_2$  is well known with two well-separated and narrow excitonic emissions, which can be attributed to neutral free excitons ( $X_0$ ) at 1.742 eV and free charged excitons (T), at 1.711 eV, which is consistent with previously reported results<sup>32</sup> (Figure 2c). By contrast, the PL spectrum of the twisted  $\text{WSe}_2/\text{WS}_2$  heterobilayer is strikingly different from that of 1L- $\text{WSe}_2$ . Figure 2c shows the PL spectrum of the  $\text{WSe}_2/\text{WS}_2$  heterobilayer with a twist angle of  $3^\circ$ , which can find that the PL spectrum of  $\text{WSe}_2/\text{WS}_2$  heterostructure has additional fine peaks (M) on the lower-energy side beside the neutral free excitons peak ( $X_0'$ ) at 1.651 eV and the trion peak ( $T'$ ) at 1.708 eV. This suggests the existence of a periodic moiré superlattice in the twisted  $\text{WSe}_2/\text{WS}_2$  heterobilayer, creating moiré traps at the interface that traps the excitons in them, modulating their energy levels and causing them to split. To further examine the influence of the moiré potential on interlayer excitons, we prepared the  $\text{WSe}_2/\text{WS}_2$  heterobilayer with different twist angles. By adjusting the twist angle, the moiré superlattice period can be tuned. With the increase of the twist angle, the moiré superlattice period decreases, resulting in an increase in the moiré potential, which modulates more exciton energies and further form moiré excitons. Figure S3 shows the PL spectra of the  $\text{WSe}_2/\text{WS}_2$  heterobilayer with twist angles of  $3^\circ$  and  $1.5^\circ$ , respectively. We focus on the  $\text{WSe}_2/\text{WS}_2$  heterobilayer with a twist angle of  $3^\circ$ . The central emission energies extracted are 1.545 eV, 1.503 eV, 1.472 eV, 1.437 eV, respectively. Compared to the  $\text{WSe}_2/\text{WS}_2$  heterobilayer with twist angles of  $1.5^\circ$ , the splitting peaks are shifted towards lower energies. This is mainly because with the twist angle increases, the depth of moiré potential increases, capturing more excitons to form the splitting peaks. Our experimental results further proved that the stack of the  $\text{WSe}_2/\text{WS}_2$  heterobilayer with different twist angles can effectively improve the moiré potential. Meanwhile, the change of these exciton peaks with the twist angle further proves that excitonic states with low-energy emissions originate from moiré excitons.

The construction of a twisted-angle  $\text{WSe}_2/\text{WS}_2/\text{WSe}_2$  heterotrilinear can form double moiré fringes, which enable highly localized moiré excitons. We performed micro-photoluminescence measurements on the  $\text{WSe}_2/\text{WS}_2/\text{WSe}_2$  heterotrilinear with a twist angle of  $3^\circ$  at 6 K under a low excitation power (Figure 2c). Compared to the  $\text{WSe}_2/\text{WS}_2$  heterobilayer with a twist angle of  $3^\circ$ , the intensity of the intralayer excitons and moiré exciton peaks in the twisted-angle  $\text{WSe}_2/\text{WS}_2/\text{WSe}_2$  heterotrilinear are increased by 3-5 times. The localization of moiré excitons in a supermoiré-induced potential trap gives rise to a sharp emission peak. To further verify the localized effects of twist angle on moiré excitons, we prepared the  $\text{WSe}_2/\text{WS}_2/\text{WSe}_2$  heterotrilinear with different twist angles. Figure 2d shows the PL spectra of the  $\text{WSe}_2/\text{WS}_2$  heterobilayer with twist angles of  $1.5^\circ$ , which can also find the same moiré excitons localization phenomenon. The considerably narrow line width of the localized moiré exciton peaks (average line width = 3.2 meV, Figure 2d, top) compared to that of the moiré exciton peaks without localization (average line width = 12.5 meV, Figure 2d, bottom). The localization of moiré excitons is mainly due to the double moiré fringes formed at the interface of the  $\text{WSe}_2/\text{WS}_2/\text{WSe}_2$  heterotrilinear, resulting in deeper and narrower moiré potential traps. In a highly confined moiré potential well can lead to an increase in the Auger recombination rate and an enhancement of exciton-exciton interactions, leading to the localization of excitons<sup>33, 34</sup>.

Temperature dependence of the integrated PL intensity provides key insight into the localized nature of moiré excitons. To further demonstrate that we observed moiré excitons in the twisted  $\text{WSe}_2/\text{WS}_2/\text{WSe}_2$  heterotrilinear, we studied the PL intensity as a function of temperature. The contour map of the temperature dependence of the PL spectra shown in Figure 3a displays the origins of additional spectral fine structures in the  $\text{WSe}_2/\text{WS}_2$  heterobilayer with a twist angle of  $3^\circ$ . Figure 3b shows the PL spectrum of the twisted  $\text{WSe}_2/\text{WS}_2$  heterobilayer at 6 K and fitted with Gaussian functions. It can be clearly found that multiple splitting peaks at 1.4 and 1.57 eV are different from the monolayer  $\text{WSe}_2$  exciton peaks, which is mainly caused by the moiré potential trapping excitons in the twisted  $\text{WSe}_2/\text{WS}_2$  heterobilayer. Figure 3c presents the PL spectra from 6 to 30 K obtained from the

horizontal line cut of the contour map. The red-shift of the PL peaks with increasing temperature are owed to the temperature-dependent bandgap shift.

At the same time, Figure 3c shows the temperature dependence of the PL intensities of the moiré excitons and the trion (T') state. With the temperature increases, The PL intensity of the moiré excitons states rapidly decreases and disappears at temperatures higher than ~30 K. This is mainly because the thermal energy is greater than the trapping potential energy, and the exciton bound state undergoes thermal dissociation assisted by thermal excitation. The experimental results can be explained by the temperature dependence of the integrated PL intensity assisted by the thermal excitation<sup>35, 36</sup>:

$$I(T) = I(0) \frac{1}{1 + A \exp\left(-\frac{E}{k_B T}\right)}$$

$I(0)$  is the PL intensity at the lowest temperature limit,  $k_B$  is the Boltzmann constant,  $A$  refers to the parameter,  $E$  is the activation energy corresponding to the depth of the moiré potential, and  $T$  is the temperature. The relationship between the PL intensity and temperature can be seen through this formula, and it can be found that the moiré potential has an influence on the thermal dissociation and thermal excitation of the exciton bound state. The moiré-trapped state has moiré potential confinement energy than the trion (T') state, so T' can be delocalized more easily with a thermally assisted process. As shown in Figure 3c, the intensity of the trion (T') PL decreases more rapidly and can no longer decompose when the temperature is greater than 20 K. The T' state exhibits a faster radiative recombination process. As a result of the confinement of the moiré potential, the PL intensity of the moiré excitons decreases relatively slowly. These findings are consistent with the previously reported results of the moiré excitons, implying that the extra peaks come from the moiré potential.

The contour map of the temperature dependence of the PL spectra shown in Figure 3d reveals the origins of additional spectral fine structures in the WSe<sub>2</sub>/WS<sub>2</sub>/WSe<sub>2</sub> heterotrilinear with a twist angle of 3°. Figure 3e show the PL spectrum of the twisted WSe<sub>2</sub>/WS<sub>2</sub>/WSe<sub>2</sub> heterotrilinear at 6 K and fitted with Gaussian functions, which can be found that multiple



splitting peaks at 1.4 and 1.6 eV are different from the  $\text{WSe}_2/\text{WS}_2$  heterobilayer exciton peaks. The intensity of the intralayer excitons and moiré exciton peaks in the twisted-angle  $\text{WSe}_2/\text{WS}_2/\text{WSe}_2$  heterotrilinear are increased by 3-5 times. The localization of moiré excitons in a supermoiré-induced potential trap gives rise to a sharp emission peak. This is mainly due to the formation of double moiré fringes at the  $\text{WSe}_2/\text{WS}_2/\text{WSe}_2$  heterotrilinear, which results in deeper and narrower moiré potential traps, leading to the localization of moiré excitons. To further prove that the localized moiré exciton states have a deeper moiré potential, we extracted the exciton peaks as a function of temperature. Figure 3f presents the PL spectra from 6 to 77 K obtained from the horizontal line cut of the contour map. The intensity of the trion ( $T'$ ) PL decreases more rapidly and can no longer decompose when the temperature is greater than 30 K. Compared to the  $\text{WSe}_2/\text{WS}_2$  heterobilayer with a twist angle of  $3^\circ$ , the PL intensity of the moiré excitons state of the  $\text{WSe}_2/\text{WS}_2/\text{WSe}_2$  heterotrilinear decreases slowly and disappears at temperatures higher than  $\sim 50$  K. Our experimental results further demonstrate that localized moiré excitons have a deeper trapping potential and require more thermal energy to delocalize the excitons.

Another important effect of the moiré potential is the excitation power dependence of the PL spectra, we investigated the power-dependent PL spectrum in the twisted  $\text{WSe}_2/\text{WS}_2/\text{WSe}_2$  heterotrilinear under 532 nm laser excitation at 6 K. Figure 4a shows the PL spectra of the  $\text{WSe}_2/\text{WS}_2/\text{WSe}_2$  heterotrilinear at different power densities at 6 K. At low excitation intensities below  $\sim 0.3$  mW, we can observe that the PL spectrum shows that the moiré excitonic peaks ( $M_1$ ,  $M_2$ ,  $M_3$ , and  $M_4$ ) dominate the spectrum. With the excitation power increases, the moiré exciton peaks at lower energy levels gradually disappear and the peak widths become larger. At the same time, we also found that with the increase of excitation power (more than 1 mW), the moiré exciton peaks changed from multiple small splitting peaks to the main peak dominated by intralayer excitons, and the intensity of high energy level ( $X'$  and  $T'$ ) peaks increased. The results indicate that at low power (less than 0.3 mW), the splitting peaks of the PL spectrum are mainly due to the capture of excitons by the moiré potential. With the increase of power, exciton filling goes from low energy level to

high energy level sequentially. The moiré flat bands are filled and gradually reach saturation, losing its modulation effect on excitons.

To further observe the evolution trend of moiré excitons with excitation power, we extracted the PL intensities of moiré exciton peaks and intralayer exciton peaks as a function of power (Figure 4b). The shapes with different colors indicate different peak positions extracted. We can find that the moiré excitons increase linearly with power at the low excitation power and quickly saturate. With the increase of power, excitons are sequentially filled from low energy level to high energy level, the moiré exciton peaks gradually disappear, and the energy is transferred to the intralayer exciton peaks of high energy level. Meanwhile, we find that the interlayer exciton peaks ( $M_1$ ,  $M_2$ ,  $M_3$ , and  $M_4$ ) blue-shift with the increase of power, which is mainly caused by repulsive dipole-dipole interactions. However, intralayer excitons do not move with the increase of power (Supplementary Fig. 4). To further distinguish intralayer excitons, we extracted the PL intensities of intralayer exciton peaks as a function of power. With the increase of power, we find that the intensity of the neutral exciton ( $X_0$ ) peak increases linearly with power, whereas the intensity of charged exciton peak ( $T'$ ) increases nonlinearly with power, which is consistent with the previous reports<sup>37</sup>.

In a twisted-angle heterojunction, an ideal moiré superlattice has  $C_3$  symmetry and it emits the same amount of co-polarized and cross-polarized light. When linearly polarized light is used to excite an ideal moiré superlattice, the direction of the linearly polarized light has no effect on the emitted light<sup>38, 39</sup>. Therefore, the linear polarization can be used to demonstrate how close the  $WSe_2/WS_2/WSe_2$  heterotrilayer is to being an ideal moiré superlattice. Figure 5a,b show the linearly polarized spectrum of the monolayer  $WSe_2$ , which can be found that the  $X_0$  exciton of the monolayer  $WSe_2$  do not change significantly with the change of the linear polarization direction  $\phi$  (Supplementary Figure S5a). This is mainly because the monolayer  $WSe_2$  has  $C_3$  symmetry and its photoluminescence does not exhibit linear polarization.

Figure 5c,d show the linear polarization dependence of the twisted, which can be found that the excitons of the twisted  $WSe_2/WS_2/WSe_2$  heterotrilayer are slightly affected by the linear polarization (Supplementary Figure S5b). In fact, the highest degree of linear

polarization in the  $\text{WSe}_2/\text{WS}_2/\text{WSe}_2$  heterotrilaier (Figure 5d) was around  $(10 \pm 8)\%$  at the emission energy of 1.689 eV. The excitons of the twisted  $\text{WSe}_2/\text{WS}_2/\text{WSe}_2$  heterotrilaier are affected by the linear polarization, which is mainly because the strain and relaxation in the heterojunction lead to the uneven distribution of the positions of the emitted co-polarized light and cross-polarized light. Moreover, the degree of linear polarization in our twisted heterojunction is much lower than that of strained heterostructures reported in the literature, indicating that the  $C_3$  symmetry is preserved in our sample<sup>40</sup>. Therefore, the shape of the moiré superlattice formed in the twisted heterojunction is fundamentally regular. In addition, an important effect of the moiré pattern is the imposition of spatially varying optical selection rules<sup>41</sup>. To verify that we are observing a moiré exciton phenomenon, we provide evidence for the existence of moiré superlattices in the twisted  $\text{WSe}_2/\text{WS}_2/\text{WSe}_2$  heterotrilaier using the alternating circularly polarized photoluminescence. Fig. 5e,f shows PL spectra of the  $\sigma^+\sigma^+$  and  $\sigma^+\sigma^-$  configurations, which can be clearly find that there is a clear cross-polarization at 1.4 eV  $\sim$  1.6 eV. The generation of this cross-polarization is mainly due to the spatial variation caused by atomic rotational symmetry, and the relative positions of atoms in different positions in real space are different, thus affecting the optical selection rule, this is in good agreement with previous reports<sup>42</sup>. This cross-polarization phenomenon provides further evidence for the existence of a moiré superlattice in our twisted-angle heterotrilaier. We also carried out density functional theory studies to confirm the existence of moiré potentials in twisted-angle heterotrilaier (Supplementary Fig. 7). The highest valence band width is only 1 meV, indicating a flat valence band behavior in the twisted  $\text{WSe}_2/\text{WS}_2/\text{WSe}_2$  moiré superlattice. These calculated results give a good understanding of the splitting peak spacing of moiré excitons observed in our experiments.

In summary, we demonstrate a new moiré superlattice system of twisted-angle 2D heterojunctions. We construct a twisted  $\text{WSe}_2/\text{WS}_2/\text{WSe}_2$  heterotrilaier via the layer degrees of freedom, forming two periodic moiré fringes. The synergy of the two moiré potentials enables the moiré excitons at the interface highly localized, manifesting as multiple sharp emission lines. Tunable local moiré excitons can be achieved by changing the rotation angle. In addition, the changes of laser power and temperature further demonstrate the localized

effect of moiré potential on excitons. Therefore, localization-enhanced moiré superlattices in twisted van der Waals heterojunctions can be manufactured with degrees of layer freedom, and these new 2D moiré superlattices provide an exciting platform for studying emerging quantum phenomena.

## Materials and Methods

**Fabrication of moiré heterostructures.** The monolayer WSe<sub>2</sub> (WS<sub>2</sub>) films were synthesized by a typical CVD growth method. The WO<sub>3</sub> (20 mg) was selected as the solid source for the one-step growth. 50 mg of Se (S) powder was placed upstream of the tube furnace. Before heating, the system was cleaned with a high-purity Ar gas and maintained for about 30 min. Then, the furnace was heated to 830 °C and kept at this temperature for 20 min. The S powder was put in the upstream region with a temperature of 190°C. H<sub>2</sub>/Ar mixture flow was used as carrier gas. After the growth, the furnace was cooled down to room temperature naturally.

The twisted WSe<sub>2</sub>/WS<sub>2</sub>/WSe<sub>2</sub> heterotrilaier were fabricated by a wet-transfer technique with a polymethyl methacrylate (PMMA) film. One layer was transferred onto the other. The top WSe<sub>2</sub> monolayer was then stacked onto the bottom monolayer with the crystal axes rotationally aligned under an optical microscope. Finally, the SHG was used to determine the rotation angle between the two monolayers, and the excitation light source of the SHG signal is a 1064 nm pulsed laser. The samples were annealed in a high vacuum at 300 °C for 3 h.

**Optical measurements.** For steady-state photoluminescence measurements, the sample was performed on the WITec Alpha 300R system and excited using a continuous-wave 532-nm laser focused to a spot size of 1.5 μm. The sample temperature was kept at 6K. The pressure of the low-temperature test system is below 10<sup>-5</sup> pa, and the temperature is cooled by compressing helium gas. When the temperature is stable at 6 K, the PL spectrum test of the sample is carried out. The model of the cryogenic refrigeration system is C04-005-044, which comes from the Cryo Industries of America.

## Acknowledgments

The authors acknowledge support from the National Natural Science Foundation of China (Grant No. 61775241), Hunan province key research and development project (Grant

No.2019GK2233), Hunan Provincial Science Fund for Distinguished Young Scholars(Grant No: 2020JJ2059), and the Youth Innovation Team (Grant No:2019012) of CSU, the Science and Technology Innovation Basic Research Project of Shenzhen (Grant No. JCYJ20190806144418859), the National Natural Science Foundation of China (Nos. 62090035 and U19A2090), the Key Program of Science and Technology Department of Hunan Province (2019XK2001, 2020XK2001). The authors are also thankful for the support of the High-Performance Complex Manufacturing Key State Lab Project, Central South University (Grant No. ZZYJKT2020-12). ZWL thanks the support from the Australian Research Council (ARC Discovery Project, DP180102976). CTW acknowledges the support from the National Natural Science Foundation of China (Grant No. 11974387) and the Strategic Priority Research Program of the Chinese Academy of Sciences (Grant No. XDB33000000). HHZ acknowledges the support from the Postdoctoral Science Foundation of China (2022M713546). The authors acknowledge the Beijing Super Cloud Computing Center (BSCC, [www.blsc.cn](http://www.blsc.cn)) for providing HPC resources that have contributed to the research results reported in this paper.

## **Author Contributions**

YPL designed and managed the project. HHZ fabricated the device and performed the Raman and PL characterizations. HHZ SFL, BW performed the low-temperature measurements. YPL, ALP, HHZ, BW, JH, ZWL, JTW and CTW provided a vital interpretation of the data. YPL, HHZ and ZWL drafted the paper. JTW and CTW provided DFT theoretical calculations and related theoretical explanations. All authors read and contributed to the revising of the manuscript.

## **Conflict of interests**

The authors declare that they have no competing interests.

## **References**

1. Cao, Y. *et al.* Correlated insulator behaviour at half-filling in magic-angle graphene superlattices. *Nature* **556**, 80–84 (2018).
2. Yang, J., Xu, R., Pei, J. *et al.* Optical tuning of exciton and trion emissions in monolayer phosphorene. *Light Sci Appl* **4**, e312 (2015).

3. Chen, G. *et al.* Evidence of a gate-tunable Mott insulator in a trilayer graphene moiré superlattice. *Nat. Phys.* **15**, 237–241 (2019).
4. Naik, M.H., Regan, E.C., Zhang, Z. *et al.* Intralayer charge-transfer moiré excitons in van der Waals superlattices. *Nature* **609**, 52–57 (2022).
5. Wang, H., Ma, S., Zhang, S. *et al.* Intrinsic superflat bands in general twisted bilayer systems. *Light Sci Appl* **11**, 159 (2022).
6. Ye, T., Li, Y., Li, J. *et al.* Nonvolatile electrical switching of optical and valleytronic properties of interlayer excitons. *Light Sci Appl* **11**, 23 (2022).
7. Zhang, C. *et al.* Interlayer couplings, Moiré patterns, and 2D electronic superlattices in MoS<sub>2</sub>/WSe<sub>2</sub> heterobilayers. *Sci. Adv.* **3**, e1601459 (2017).
8. Sharpe, A. L. *et al.* Emergent ferromagnetism near three-quarters filling in twisted bilayer graphene. *Science* **365**, 605–608 (2019).
9. Chen, G. *et al.* Tunable correlated Chern insulator and ferromagnetism in a moiré superlattice. *Nature* **579**, 56–61 (2020).
10. White, S.J.U., Yang, T., Donschuk, N. *et al.* Electrical control of quantum emitters in a Van der Waals heterostructure. *Light Sci Appl* **11**, 186 (2022).
11. Polshyn, H. *et al.* Electrical switching of magnetic order in an orbital Chern insulator. *Nature* **588**, 66–70 (2020).
12. Regan, E. C. *et al.* Mott and generalized Wigner crystal states in WSe<sub>2</sub>/WS<sub>2</sub> moiré superlattices. *Nature* **579**, 359–363 (2020).
13. Xian, L., Kennes, D. M., Tancogne-Dejean, N., Altarelli, M. & Rubio, A. Multiflat bands and strong correlations in twisted bilayer boron nitride: doping-induced correlated insulator and superconductor. *Nano Lett.* **19**, 4934–4940 (2019).
14. Tang, Y. *et al.* Simulation of Hubbard model physics in WSe<sub>2</sub>/WS<sub>2</sub> moiré superlattices. *Nature* **579**, 353–358 (2020).
15. Cao, Y. *et al.* Unconventional superconductivity in magic-angle graphene superlattices. *Nature* **556**, 43–50 (2018).
16. Chen, D., Lian, Z., Huang, X. *et al.* Tuning moiré excitons and correlated electronic states through layer degree of freedom. *Nat Commun* **13**, 4810 (2022).
17. Wu, B., Zheng, H., Li, S. *et al.* Evidence for moiré intralayer excitons in twisted

- WSe<sub>2</sub>/WSe<sub>2</sub> homobilayer superlattices. *Light Sci Appl* **11**, 166 (2022).
18. Huang, D., Choi, J., Shih, CK. *et al.* Excitons in semiconductor moiré superlattices. *Nat. Nanotechnol.* **17**, 227–238 (2022).
  19. Quan, J., Linhart, L., Lin, ML. *et al.* Phonon renormalization in reconstructed MoS<sub>2</sub> moiré superlattices. *Nat. Mater.* **20**, 1100–1105 (2021).
  20. Kim, J., Ko, E., Jo, J. *et al.* Anomalous optical excitations from arrays of whirlpooled lattice distortions in moiré superlattices. *Nat. Mater.* **21**, 890–895 (2022).
  21. Qiu, Z., Holwill, M., Olsen, T. *et al.* Visualizing atomic structure and magnetism of 2D magnetic insulators via tunneling through graphene. *Nat Commun* **12**, 70 (2021).
  22. Yu, H., Liu, G.-B., Tang, J., Xu, X., Yao, W. Moiré Excitons: From Programmable Quantum Emitter Arrays to Spin-Orbit-Coupled Artificial Lattices. *Sci. Adv.* **3**, No. e1701696 (2017).
  23. Wu, F., Lovorn, T., Macdonald, A. H. Theory of Optical Absorption by Interlayer Excitons in Transition Metal Dichalcogenide Heterobilayers. *Phys. Rev. B: Condens. Matter Mater. Phys.* **97**, 035306 (2018).
  24. Lamas-Linares, A., Howell, J. C., Bouwmeester, D. Stimulated Emission of Polarization-Entangled Photons. *Nature* **412**, 887-890 (2001).
  25. Karni, O., Barré, E., Pareek, V. *et al.* Structure of the moiré exciton captured by imaging its electron and hole. *Nature* **603**, 247–252 (2022).
  26. Turunen, M., Brotons-Gisbert, M., Dai, Y. *et al.* Quantum photonics with layered 2D materials. *Nat Rev Phys* **4**, 219–236 (2022).
  27. Zhang, L., Wu, F., Hou, S. *et al.* Van der Waals heterostructure polaritons with moiré-induced nonlinearity. *Nature* **591**, 61–65 (2021).
  28. Seyler, K.L., Rivera, P., Yu, H. *et al.* Signatures of moiré-trapped valley excitons in MoSe<sub>2</sub>/WSe<sub>2</sub> heterobilayers. *Nature* **567**, 66–70 (2019).
  29. Sergeev, A.A., Pavlov, D.V., Kuchmizhak, A.A. *et al.* Tailoring spontaneous infrared emission of HgTe quantum dots with laser-printed plasmonic arrays. *Light Sci Appl* **9**, 16 (2020).
  30. Zhao, S., Wang, E., Üzer, E.A. *et al.* Anisotropic moiré optical transitions in twisted monolayer/bilayer phosphorene heterostructures. *Nat Commun* **12**, 3947 (2021).

31. Misa Anđelkovic. *et al.* Double Moiré with a Twist: Supermoiré in Encapsulated Graphene. *Nano Lett.* **20**, 979–988 (2020).
32. Ye, Z., Waldecker, L., Ma, E.Y. *et al.* Efficient generation of neutral and charged biexcitons in encapsulated WSe<sub>2</sub> monolayers. *Nat Commun* **9**, 3718 (2018).
33. Pietryga, J. M., Zhuravlev, K. K., Whitehead, M., Klimov, V. I., Schaller, R. D. Evidence for barrierless Auger recombination in PbSe nanocrystals: A pressure-dependent study of transient optical absorption. *Phys. Rev. Lett.* **101**, 217401(2008).
34. Robel, I., Gresback, R., Kortshagen, U., Schaller, R. D., Klimov, V. I. Universal size-dependent trend in Auger recombination in direct-gap and indirect-gap semiconductor nanocrystals. *Phys. Rev. Lett.* **102**, 177404 (2009).
35. Shibata, H. Negative Thermal Quenching Curves in Photoluminescence of Solids. *Jpn. J. Appl. Phys.* **37**, 550 (1998).
36. Fang, Y., Wang, L., Sun, Q. *et al.* Investigation of temperature-dependent photoluminescence in multi-quantum wells. *Sci Rep* **5**, 12718 (2015).
37. Paur, M., Molina-Mendoza, A.J., Bratschitsch, R. *et al.* Electroluminescence from multi-particle exciton complexes in transition metal dichalcogenide semiconductors. *Nat Commun* **10**, 1709 (2019).
38. Yu, H., Liu, G. B., Tang, J., Xu, X., Yao, W. Moiré excitons: From programmable quantum emitter arrays to spin-orbit-coupled artificial lattices. *Sci. Adv.* **3**, e1701696 (2017).
39. Wu, F., Lovorn, T., MacDonald, A. H. Theory of optical absorption by interlayer excitons in transition metal dichalcogenide heterobilayers. *Phys. Rev. B: Condens. Matter Mater. Phys.* **97**, 035306 (2018).
40. Bai, Y., *et al.* Excitons in strain-induced one-dimensional moiré potentials at transition metal dichalcogenide heterojunctions. *Nat. Mater.* **19**, 1068-1073 (2020).
41. Yu, H., Liu, G.-B., Tang, J., Xu, X. & Yao, W. Moiré excitons: From programmable quantum emitter arrays to spin-orbit-coupled artificial lattices. *Sci. Adv.* **3**, e1701696 (2017).
42. Tran, K., Moody, G., Wu, F. *et al.* Evidence for moiré excitons in van der Waals heterostructures. *Nature* **567**, 71–75 (2019).



## Figures and Captions

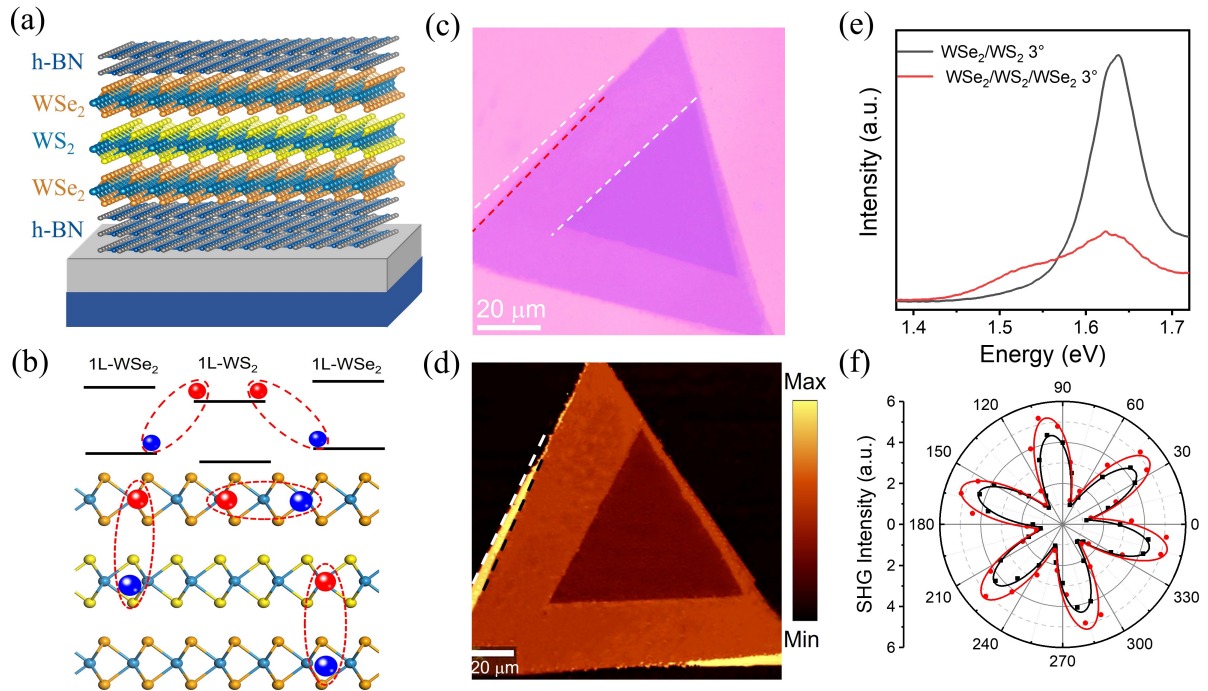


**Fig. 1** Moiré superlattice and interlayer exciton emission in a  $\text{WSe}_2/\text{WS}_2/\text{WSe}_2$  heterotrilayer. (a) Schematic illustration of a vertically stacked  $\text{WSe}_2/\text{WS}_2/\text{WSe}_2$  twisted-angle heterotrilayer with hexagonal boron nitride (h-BN) on a  $\text{SiO}_2/\text{Si}$  substrate. The twisted  $\text{WSe}_2/\text{WS}_2/\text{WSe}_2$  heterotrilayer is a system composed of two-layer  $\text{WSe}_2$  and one-layer  $\text{WS}_2$ . The top and bottom sheets are aligned, and the middle sheet is rotated by a  $\theta$  angle of approximately  $3^\circ$  relative to the other two sheets. (b) Schematic diagram of the alignment of type II bands in the  $\text{WSe}_2/\text{WS}_2/\text{WSe}_2$  heterotrilayer. The energy levels are represented by black solid lines, and the interlayer excitons and intralayer excitons are marked by dashed ellipses. (c) Optical microscopy image of the  $\text{WSe}_2/\text{WS}_2/\text{WSe}_2$  heterotrilayer, with the heterojunctions encapsulated with flakes of BN (Supplementary Fig. 1). (d) Raman mapping of a twisted  $\text{WSe}_2/\text{WS}_2/\text{WSe}_2$  heterotrilayer. (e) The PL spectra of heterojunctions with different layers at room temperature. (f) Measured and fitted the SHG signals of the top  $\text{WSe}_2$  monolayer and middle  $\text{WS}_2$  monolayer regions of the sample, which confirm the  $3^\circ$  twist angle between the top and middle layers.

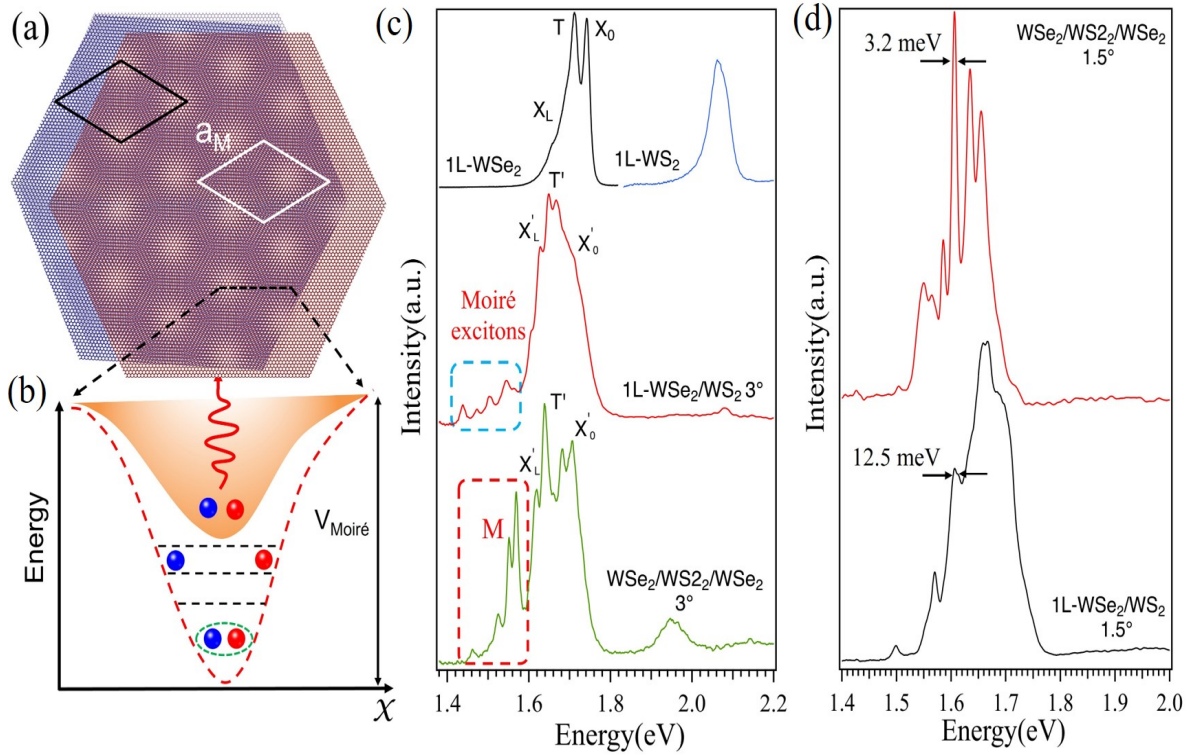


**Fig. 2 Moiré exciton localization in a twisted heterotrilaier.** (a) Schematics of moiré superlattices formed in the twisted  $\text{WSe}_2/\text{WS}_2/\text{WSe}_2$  heterotrilaier. (b) The moiré superlattice leads to a periodic moiré potential in the twisted  $\text{WSe}_2/\text{WS}_2/\text{WSe}_2$  heterotrilaier, which can trap excitons in the moiré traps. The deeper the moiré potential, the more excitons can be trapped. (c) Representative PL spectra of 1L- $\text{WSe}_2$ , 1L- $\text{WS}_2$ ,  $\text{WSe}_2/\text{WS}_2$  heterobilayer with a twist angle of  $3^\circ$  and the  $\text{WSe}_2/\text{WS}_2/\text{WSe}_2$  heterotrilaier with a twist angle of  $3^\circ$ . The PL intensity of the heterostructure is multiplied by a factor of three to facilitate comparison with the PL spectrum of 1L- $\text{WSe}_2$ . The T and  $X_0$  peaks are assigned to emissions from the trion and exciton of the 1L- $\text{WSe}_2$ , respectively. The low-energy additional peaks representing moiré excitons are indicated by the red dotted box (M). (d) Representative PL spectra of  $\text{WSe}_2/\text{WS}_2$  heterobilayer with a twist angle of  $1.5^\circ$  and the  $\text{WSe}_2/\text{WS}_2/\text{WSe}_2$  heterotrilaier with a twist angle of  $1.5^\circ$ . Line widths of moiré excitons of 12.5 meV and 3.2 meV are obtained for  $\text{WSe}_2/\text{WS}_2$  heterobilayer and the  $\text{WSe}_2/\text{WS}_2/\text{WSe}_2$  heterotrilaier.

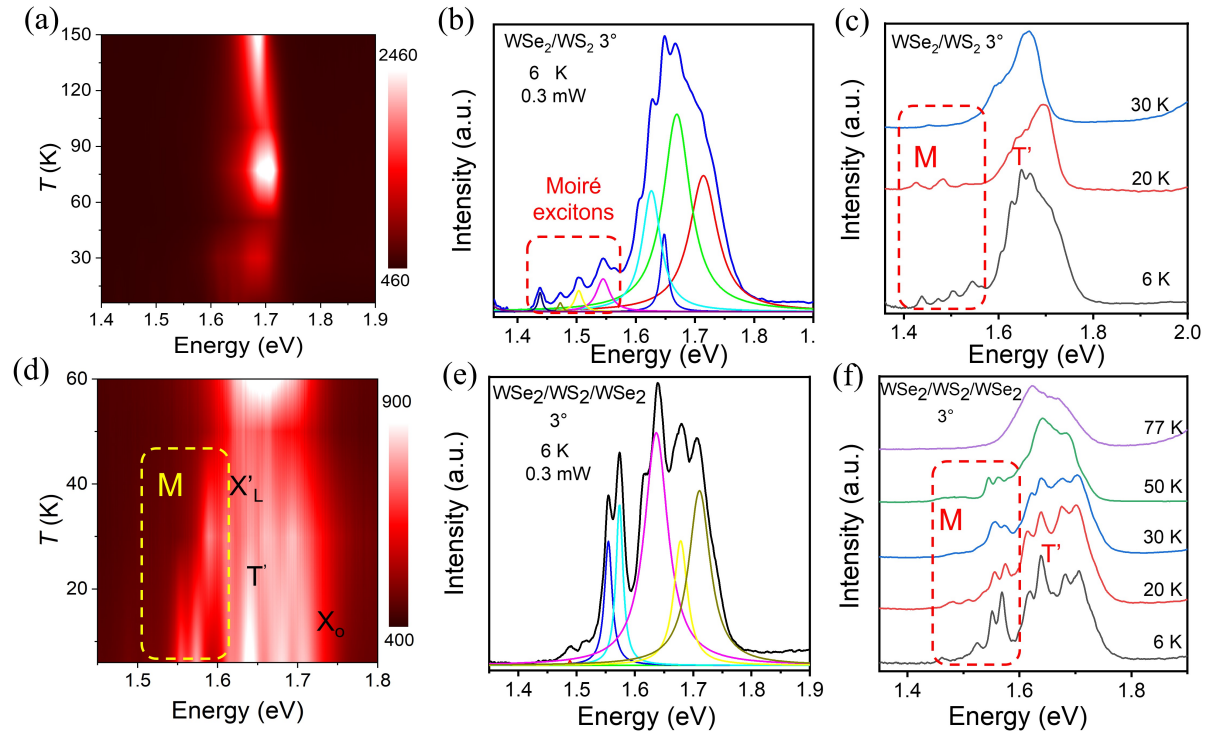


**Fig. 3 Temperature dependence of moiré excitons in the twisted  $\text{WSe}_2/\text{WS}_2/\text{WSe}_2$  heterotrilinear.** (a, b) Contour plot of the temperature-dependent PL in the  $\text{WSe}_2/\text{WS}_2$  heterobilayer with a twist angle of  $3^\circ$ . PL spectrum of  $\text{WSe}_2/\text{WS}_2$  heterobilayer at 6 K under an excitation power density of 0.3 mW extracted from the contour plot. (c) The normalized PL spectra of the twisted  $\text{WSe}_2/\text{WS}_2$  heterobilayer with a twist angle of  $3^\circ$  at various temperatures ranging from 6 to 30 K. (d, e) Contour plot of the temperature-dependent PL in the  $\text{WSe}_2/\text{WS}_2/\text{WSe}_2$  heterotrilinear with a twist angle of  $3^\circ$ . The PL spectrum shows a splitting phenomenon at 6 K under an excitation power density of 0.3 mW extracted from the contour plot. (f) The normalized PL spectra of the twisted  $\text{WSe}_2/\text{WS}_2/\text{WSe}_2$  heterotrilinear with twist angle of  $3^\circ$  at various temperatures ranging from 6 to 77 K.

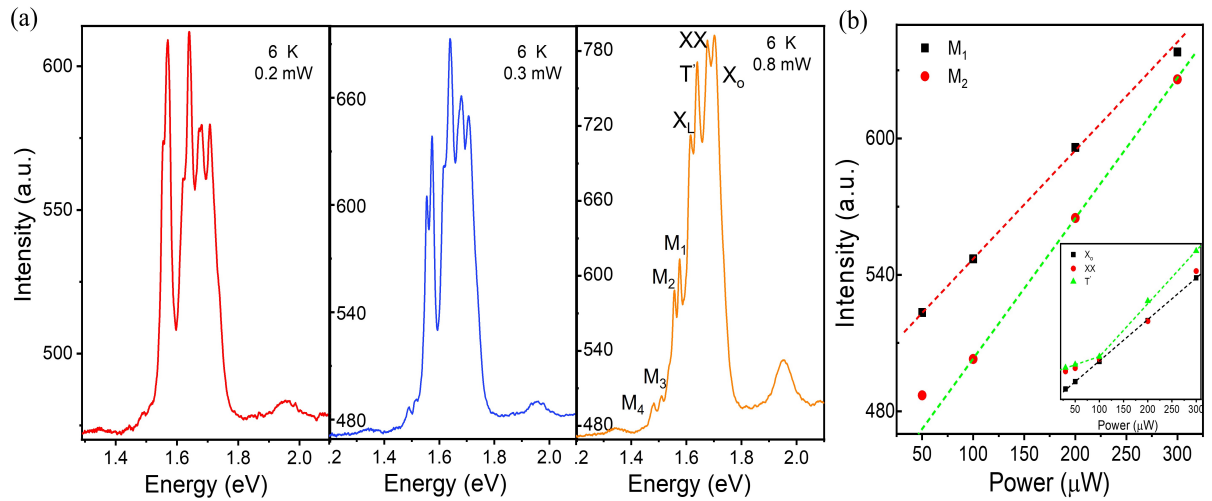


**Fig. 4 Power-dependence of moiré excitons in twisted  $\text{WSe}_2/\text{WS}_2/\text{WSe}_2$  heterotrilayer.** (a) PL spectra of the twisted  $\text{WSe}_2/\text{WS}_2/\text{WSe}_2$  heterotrilayer as a function of excitation power under 532 nm laser excitation at 6 K. (b) The PL intensity of  $M_1$ ,  $M_2$  peaks as a function of excitation power under 532 nm laser excitation at 6 K. The inset shows the PL intensity of the  $T$ ,  $XX$  and  $X_0$  peaks as a function of excitation power.

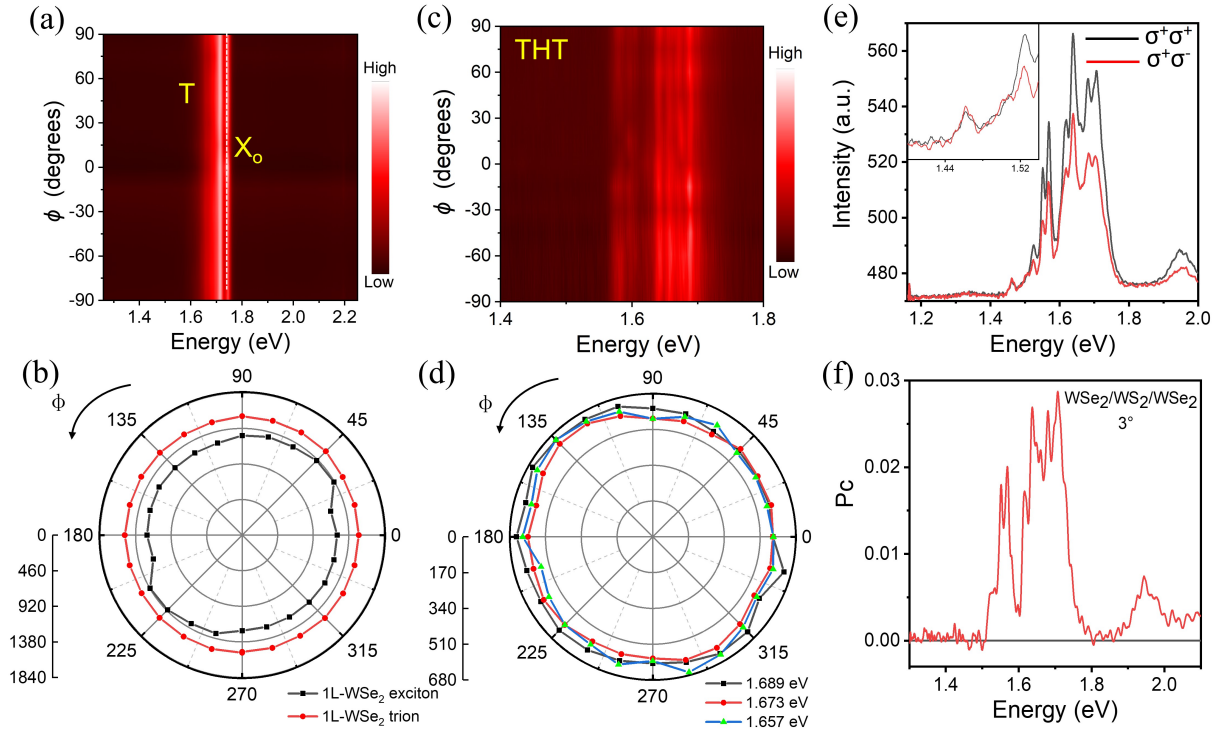


**Fig. 5 Valley polarization and linear polarization of trapped excitons in WSe<sub>2</sub>/WS<sub>2</sub>/WSe<sub>2</sub> heterotrilyer.** (a, b) Line tangent point of exciton energy in the monolayer WSe<sub>2</sub> as a function of the angle  $\phi$  between the half-wave plate and linear polarizer. (c, d) Linear polarization spectra of the twisted WSe<sub>2</sub>/WS<sub>2</sub>/WSe<sub>2</sub> heterotrilyer with a twist angle of 1.5°. (e, f) Circularly polarized photoluminescence spectrum for  $\sigma^+$  and  $\sigma^-$  excitation of the WSe<sub>2</sub>/WS<sub>2</sub>/WSe<sub>2</sub> heterotrilyer with a twist angle of 3° at 6 K. The relationship between the degree of circular polarization and the emission wavelength are obtained from the spectrum of 5(e).

## Supplementary Files

This is a list of supplementary files associated with this preprint. Click to download.

- [SupplementaryMaterials.pdf](#)